Out-of-plane spin-orientation dependent magnetotransport properties in the anisotropic helimagnet $Cr_{1/3}NbS_2$

Alexander C. Bornstein,[1] Benjamin J. Chapman,[1] Nirmal J. Ghimire,[2,3,*] David G. Mandrus,[2,3,4] David S. Parker,[3] and Minhyea Lee[1,†]

[1]*Department of Physics, University of Colorado, Boulder, Colorado 80309, USA*
[2]*Department of Physics and Astronomy, The University of Tennessee, Knoxville, Tennessee 37996, USA*
[3]*Materials Science and Technology Division, Oak Ridge National Laboratory, Oak Ridge, Tennessee 37831, USA*
[4]*Department of Materials Science and Engineering, The University of Tennessee, Knoxville, Tennessee 37996, USA*

(Received 11 December 2014; revised manuscript received 3 April 2015; published 6 May 2015)

Understanding the role of spin-orbit coupling (SOC) has been crucial for controlling magnetic anisotropy in magnetic multilayer films. It has been shown that electronic structure can be altered via interface SOC by varying the superlattice structure, resulting in spontaneous magnetization perpendicular or parallel to the plane. In lieu of magnetic thin films, we study the similarly anisotropic helimagnet $Cr_{1/3}NbS_2$ where the spin-polarization direction, controlled by the applied magnetic field, can modify the electronic structure. As a result, the direction of spin polarization can modulate the density of states and in turn affect the in-plane electrical conductivity. In $Cr_{1/3}NbS_2$, we found an enhancement of in-plane conductivity when the spin polarization is out-of-plane as compared to in-plane spin polarization. This is consistent with the increase in density of states near the Fermi energy at the same spin configuration, found from first-principles calculations. We also observe unusual field dependence of the Hall signal in the same temperature range. This is unlikely to originate from the noncollinear spin texture but rather further indicates strong dependence of electronic structure on spin orientation relative to the plane.

DOI: 10.1103/PhysRevB.91.184401 PACS number(s): 75.30.Gw, 75.70.Tj, 71.20.−b

Despite the fact that its typical energy scale in 3*d* ferromagnetic metals is small compared to other relevant scales, such as band widths, spin-orbit coupling (SOC) mixes the nature of the spin and orbital components of the Bloch state in a nontrivial way and leads to a variety of electrical transport phenomena, e.g., the anomalous Hall effect (AHE), anisotropic magnetoresistance (AMR), and the planar Hall effect. In addition, the recent work on noncollinear magnetically ordered states and the related topological Hall effect (THE) [1–3] not only has renewed the pivotal role of SOC through the Dzyaloshinskii-Moriya (DM) interaction [4–6], but also has presented a possibility to employ these findings for functional components in magnetic devices [7,8]. Noncollinear magnetic ordering is also suggested to possibly manifest spin-orbit coupling in a complex manner through the DM interaction [6,9,10]. Consequently, the modification of electronic structure by spin-orbit coupling is expected to make in-plane electrical transport sensitive to the magnetization orientation relative to the plane.

$Cr_{1/3}NbS_2$ has a layered crystalline structure in which 3*d* transition-metal Cr atoms are intercalated in the hexagonal $2H$-type NbS_2 matrix as trivalent ions and magnetically order at $T_C = 133$ K. The ferromagnetic layers of Cr^{3+} lie coplanar with the crystallographic *ab* planes, and the magnetic helix propagates along the *c* axis with a long pitch of 48 nm, corresponding to 40 unit cells [11]. Its helimagnetic ordering is attributed to the DM interaction, which originates from a broken inversion symmetry shared by all members of space group $P6_322$ [11–13]. With the application of a magnetic field (H) along the *ab* plane, i.e., perpendicular to the helical axis, ferromagnetic domains are created between the winds of the helix, increasing the length of the magnetic unit cell and forming the chiral soliton lattice phase [14]. As the field is increased, all spins become polarized at $H_p^{ab} = 0.18$ T. Alternatively, when H is applied along the *c* axis, i.e., along the direction of the helical wave vector, the helices smoothly evolve through a conical state. The conical angle decreases with increasing H until polarization at $H_p^c = 2.5$ T [11,13]. Its electrical conduction is quai-two dimensional: The electrical resistivity measured with current flowing along the *c* axis is on the order of 10^1–10^2 times larger than with current on the *ab* plane [11,15]. In this regard, $Cr_{1/3}NbS_2$ displays similar magnetic and structural anisotropies as fabricated planar devices.

So far, SOC in magnetic multilayers or a superlattice has been studied intensively in terms of engineering the electronic structure in order to control the spontaneous magnetic anisotropy [16–21]. Here, we demonstrate the reverse process in a similarly anisotropic layered system $Cr_{1/3}NbS_2$ such that the spin-polarization direction controlled by the applied magnetic field alters the electronic structure via SOC. For spin polarization along the *c* axis, this results in enhanced electrical conductivity by increasing the density of states (DOS) near the Fermi surface as supported by our first-principles calculations. This observation is the most prominent for temperatures $T < T_A$; T_A is the temperature scale below which spin-disorder scattering contributes negligibly to the resistance and is empirically determined from the temperature dependence of the magnetoresistance (MR). Surprisingly, roughly the same temperature scale of T_A was found in the transverse Hall resistivity and is consistent with the onset

*Current address: Los Alamos National Laboratory, Los Alamos, New Mexico.
†minhyea.lee@colorado.edu

of deviation from Bloch's $T^{3/2}$ law for magnetization [13]. Although T_A is a crossover temperature and is not sharply defined, it corresponds to the energy scale associated with modifications of the electronic structure and is thus a useful quantity to estimate.

Single crystals of $Cr_{1/3}NbS_2$ were grown by vapor transport (see Ref. [11] for details on growth and sample characterization). Crystals from two different batches were used in this study and show slightly different T_C's of 120 and 133 K but otherwise exhibit very little qualitative difference in the T and H dependences of both electrical and magnetic measurements. All the data presented in this paper are from the sample with $T_C = 133$ K. Samples from both batches were characterized with x-ray diffraction for the crystalline structure and small-angle neutron scattering to verify the helimagnetic ground state [22]. Magnetization was measured in a superconducting quantum interference device (SQUID) magnetometer. Electrical transport properties were studied using standard four-probe measurements on samples with typical areas of $\approx 2 \times 0.3$ mm^2 and thicknesses of $\approx$20–70 μm. Electrical contacts, made by silver paint, had typical contact resistance less than 1 Ω. Rotation of the sample in a field was performed by a homebuilt rotation probe, which was inserted in a superconducting split coil magnet. For transport measurements, currents of 2–4 mA were applied on the ab plane. We used small wedges made of stycast epoxy with various angles to mount the samples under an angled magnetic field in magnetization measurements. For the Hall measurement, we checked the uniformity of the current flow by using multiple sets of electric contacts within a sample. The Hall data are antisymmetrized in order to remove the magnetoresistance component caused by a slight misalignment of the contacts.

The measurement is configured such that the flow of current lies within the crystallographic ab plane, whereas the saturated magnetization sweeps the out-of-plane polar angle from $\theta_H = 0^\circ$ to 90° [see the inset of Fig. 2(a)]. This corresponds to the out-of-plane anisotropic magnetoresistance configuration as shown in Refs. [23,24]. It is distinct from the typical AMR configuration where both current and magnetization lie within the film plane [25]. Note that the direction of current *always* remains within the ab plane and therefore, when $\theta_H = 90^\circ$ the current is parallel to H.

First, we plot the in-plane resistivities (ρ) as a function of H for $\theta_H = 0^\circ$ (thick lines) and $\theta_H = 90^\circ$ (thin lines) at different fixed temperatures (T) in Figs. 1(a) and 1(b). Figure 1(c) summarizes the T dependence of the in-plane MR, defined as $\Delta\rho/\rho_0 = [\rho(H,\theta_H) - \rho_0]/\rho_0$ with $\rho_0 = \rho(H = 0)$ at $\mu_0 H = 7$ T where all of the spins are polarized along either orientation of H. The discrepancy of the in-plane MR between the two orientations is most striking at 2 K where the reduction of MR with out-of-plane magnetization is three times larger than with in-plane magnetization. We will come back to this below. Also the H independent resistivity values in $H > H_p^c$ and $H > H_p^{ab}$ for both H directions imply that all spins are polarized and the contribution of spin-disorder induced scattering is very little.

As T increases, this trend reverses around $T_A \approx 50$ K, and $\rho(\theta_H = 0^\circ, H)$ becomes higher in the entire H range. T_A is empirically determined from the temperature at which $\rho(\theta_H = 0^\circ, H_p^c)$ is no longer smaller than $\rho(\theta_H = 90^\circ)$ as shown in Fig. 1(c). In $T > T_A$, the resistivity discrepancy between the two spin polarizations is overwhelmed by spin-disorder scattering-induced resistance. This is also clear from the H dependence of the two resistivities that are parallel to each other in $T > T_A$ in Fig. 1(b).

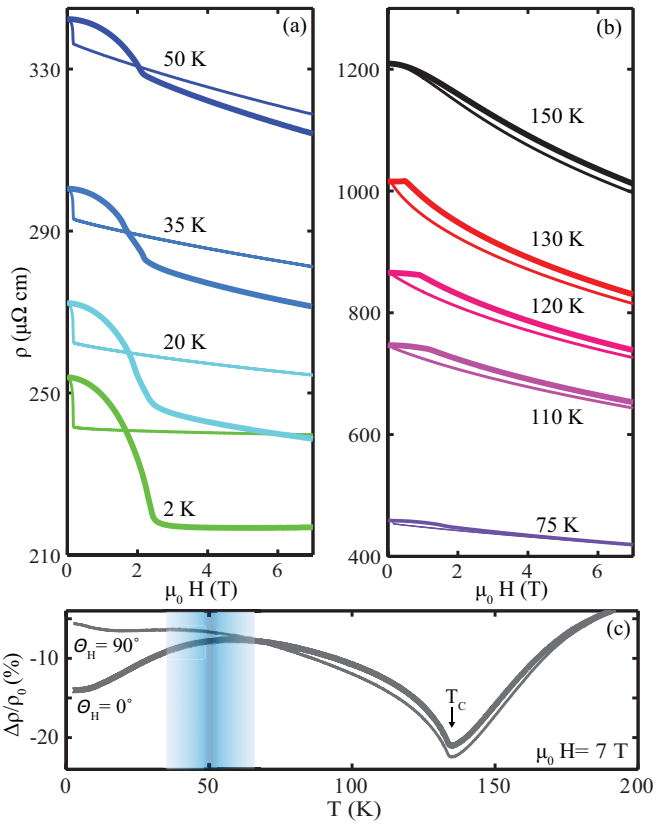

FIG. 1. (Color online) (a) and (b) In-plane resistivity ρ as a function of H in two different orientations: $\theta_H = 0^\circ$ (thick lines) and $\theta_H = 90^\circ$ (thin lines) at fixed T's (a) $T \leqslant 50$ K and (b) $T \geqslant 75$ K. At each T, H_p^c is clearly visible in both panels but in (b) H_p^{ab} is hard to identity because of the large y-axis scale. (c) The normalized in-plane magnetoresistance (MR) $\Delta\rho/\rho_0 = [\rho(H) - \rho_0]/\rho_0$ with $\rho_0 = \rho(H = 0)$ as a function of T measured at $\mu_0 H = 7$ T. $T_C = 133$ K is marked with an arrow. Blurred blue line is centered at $T_A = 52$ K, which is determined from the temperature at which $\rho(\theta_H = 0, H_p^c)$ is no longer smaller than $\rho(\theta_H = 90^\circ)$. However, since we intend T_A to indicate an approximate T scale above which the difference between the two MRs diminishes, we refer to $T_A \approx 50$ K in the main text.

The out-of-plane polarization field H_p^c is clearly identified up to T_C as is H_p^{ab}, although the scale of the axes makes it hard to identify in Fig. 1(b). At any given T, the lower polarization field for $\theta_H = 90^\circ$ indicates a more effective suppression of spin disorder for the same strength of H. This also gives rise to a lower ρ value in the entire H range for high T's. The similar rate of reduction of ρ at higher T, which makes the two curves at each temperature almost parallel, implies that their H dependence is attributed to the suppression of spin disorder.

In Fig. 2(a) we plot the magnetization along the H direction ($M_\parallel$) as a function of H for different θ_H's at $T = 5$ K $\ll T_C$. The polarization fields ($H_p^{\theta_H}$) are clearly visible, indicated with vertical lines and with arrows for both end angles of

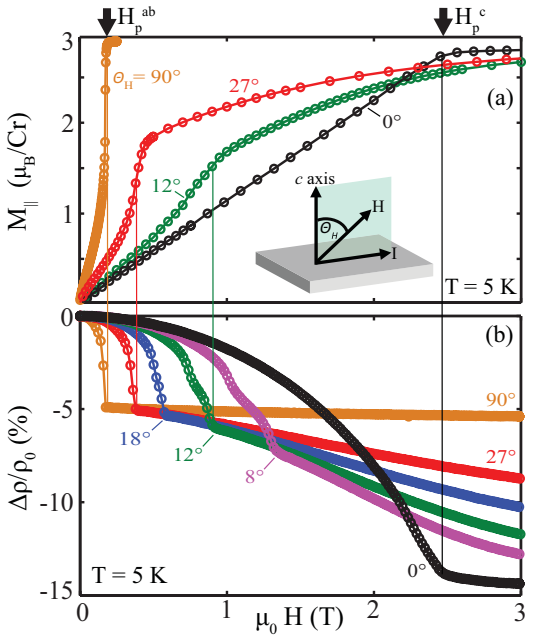

FIG. 2. (Color online) (a) The magnetization component parallel to the applied magnetic field ($M_\parallel$) as a function of H at different angle θ_H's at $T = 5$ K. The measurement configuration is shown in the inset. (b) In-plane MR as a function of H oriented at angle θ_H and $T = 5$ K. Vertical lines mark the polarization field ($H_p^{\theta_H}$) at a given θ_H. At intermediate angles, all spins are polarized at $H_p^{\theta_H}$ but are not yet aligned along the H direction [26].

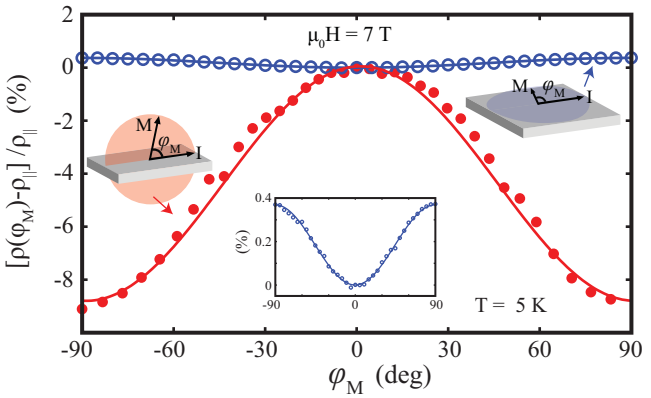

FIG. 3. (Color online) In-plane MR at $\mu_0 H = 7$ T, normalized with $\rho_\parallel(\varphi_M = 0,\ \mu_0 H = 7\ \text{T})$, where φ_M denotes the angle between the current and M both in-plane (open) and out-of-plane (closed circle) as shown in the sketches. Note the amplitude of out-of-plane AMR is 23 times larger than in-plane AMR. The angular dependences for both cases are found to be $\propto \cos^2 \varphi_M$, which is displayed in the solid lines. The inset is a plotted in-plane AMR with a magnified y axis.

$\theta_H = 0^\circ$ and 90°. It occurs at fields well approximated by $H_p^{\theta_H} \simeq \frac{H_p^{ab}}{\sin\theta_H}$ [26]. The rapid rise in magnetization observed at large angles, e.g., $\theta_H = 90^\circ$ or 27°, indicates a phase transition from the chiral soliton lattice to the ferromagnetic ordering. At intermediate angles, the rise at $H_p^{\theta_H}$ is not as rapid as at $\theta_H = 90^\circ$. Although all spins are polarized when $H = H_p^{\theta_H}$ at these angles, they are not yet aligned with the direction of H but remain closer to the ab plane. Upon increasing H more, the polarized spins collectively rotate until they eventually align with H. This results in the gradual rise of $M_\parallel$ in $H > H_p^{\theta_H}$ toward the saturated value, which is ascribed to the competition between the Zeeman and the magnetic anisotropy energies [26].

In Fig. 2(b), we compare this with the in-plane MR. At $\theta_H = 90^\circ$, the reduction in MR by 5.6% indicates a decrease in spin scattering as the helical ordering becomes polarized along H. A clear kink denotes the spin-polarization field H_p^{ab}. This domelike shape is commonly observed in other helimagnets for the same reason [27,28]. Once the spins completely polarize within the plane ($H > H_p^{ab}$), there is little variation in MR with H, which ensures that the contribution of the spin-disorder-induced MR is negligible. It is worth pointing out that $\Delta\rho/\rho_0$ at $\theta_H = 90^\circ$ bears great similarity in both H dependence and magnitude to that of the interlayer MR, i.e., the MR when I is applied along the c axis and H is in the ab plane, reported in Ref. [15].

When θ_H approaches 0, upon increasing H, the MR decreases much slower initially but eventually surpasses the in-plane value, reaching down to 14.1%, almost three times more reduction than $\theta_H = 90^\circ$. This reduction is remarkable compared to the variation found in typical traditional AMR phenomena, which are only a few tenths to a couple of percent at most [25]. Although slightly larger than a couple of percent out-of-plane AMR values have been reported in magnetic thin-film systems [23], it is attributed to the reduction in spin scattering due to the geometrical size and texture of the films. It is only very recent that the interface effect between adjacent magnetic and nonmagnetic films was identified for a possible source of the out-of-plane AMR effect, yet the reported size is less than 1% [24].

For $\theta_H = 8^\circ$ and 12° there is another kink in the MR, appearing in the range of H where the phase transition from chiral soliton lattice to ferromagnetic ordering occurs [15]. This finite width of the transition, only occurring for angles close to the c axis, is believed to be caused by the formation of multiple domains undergoing the transition at slightly different fields as also seen in $M_\parallel(H)$ of Fig. 2(a). Although these kinks indicate a great sensitivity of the electrical transport to changes in the spin structure, it does not account for the continued decrease in MR in $H > H_p^{\theta_H}$.

To have a better understanding of this spin-orientation dependent in-plane MR, we examine the AMR effect in both in-plane and out-of-plane rotations of the applied field. Schematics of the measurement are shown in the insets of Fig. 3. In the main panel, both in-plane and out-of-plane angular dependences of the in-plane resistivity normalized with $\rho_\parallel = \rho(\varphi_M = 0,\ \mu_0 H = 7\ \text{T})$ are plotted, where φ_M denotes the angle between M and I (see Supplemental Material [29]). In both cases, rotation of the magnetization gives rise to $\cos^2 \varphi_M$ angular dependences indicated with solid lines. However, the normalized AMR oscillation amplitude for the out-of-plane MR is larger by 23 times than the in-plane one; +0.4% and −9.1% change relative to $\rho_\parallel$ for in-plane and out-of-plane, respectively. Note the different sign indicates the most reduced resistivity occurs when $M \parallel I$ for in-plane

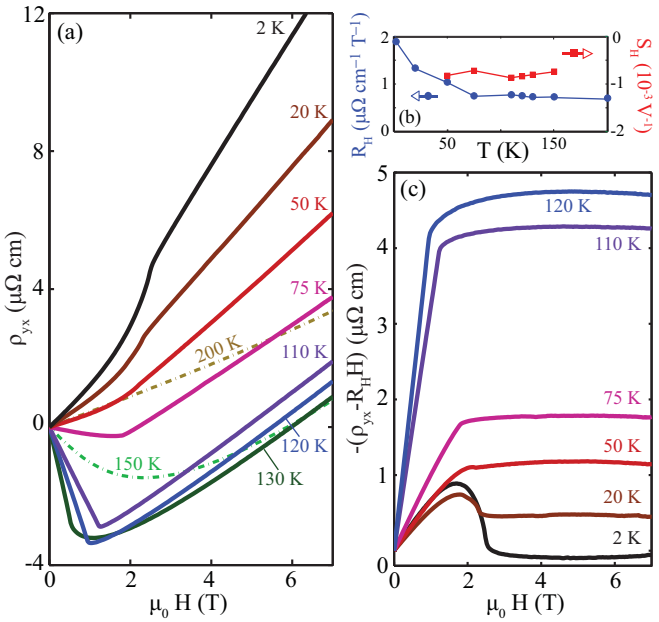

FIG. 4. (Color online) (a) H dependence of ρ_{yx} at various T's below (solid lines) and above (broken lines) T_C. Peculiar concave H dependence occurs only in $T < T_A \approx 50$ K. Since $H \parallel c$, all spins get *smoothly* polarized along the c axis via the helical and conical states as H increases. (b) The ordinary (R_H) and anomalous (S_H) Hall coefficients, determined from fits of ρ_{yx}. Above T_A, both R_H and S_H are independent of T. Below T_A, the fit no longer works, and S_H cannot be obtained in a reliable way. R_H is extracted from $\mu_0 H > 3$ T where ρ_{yx} is linear to H. (c) H dependence of ρ_{yx} less the ordinary Hall effect (OHE). AHE contribution decreases as T is lowered and is replaced with the humplike feature in $T < T_A$, which has very little resemblance with $M(H)$. The curve for 50 K displays a little dip before becoming flat, displaying the crossover between the humplike shape and the AHE component.

and $M \perp I$ for out-of-plane. This out-of-plane AMR effect should also be distinguished from giant magnetoresistance of magnetic multilayers in which the saturated MRs remain the same for both orientations [30].

Finally, we examine the Hall effect which is measured with H applied along the c axis ($\theta_H = 0$). This configuration matches those in which a THE was observed in other helimagnets, e.g., with H along the helical axis [28]. Figure 4(a) shows field sweeps of the Hall resistivity (ρ_{yx}) at various fixed T's. At low temperatures, an unexpected H dependence of ρ_{yx} emerges, characterized by the pronounced concave curvature for $0 < H < H_p^c$. As shown in Fig. 4(c), this peculiar dependence is more obvious after subtracting the ordinary Hall contribution as described in the forthcoming analysis. Note that this behavior emerges below $T_A \approx 50$ K, coinciding with the emergence of the MR discrepancy described above.

For $T > T_A$, the Hall signal exhibits archetypical anomalous Hall behavior, empirically expressed as $\rho_{yx}(H) = \mu_0 R_H H + \mu_0 R_s M$, where μ_0 is the vacuum permeability, R_H is the normal Hall coefficient, and R_s is the anomalous Hall coefficient. The first and second terms correspond to the OHE and the AHE, respectively. As T decreases, the AHE signal becomes visible at $T = 150$ K and grows more prominent through T_C where it is marked by a sharp kink at $H = H_p^c$. From the shape of the curves R_S has the opposite sign as R_H. In the limit of the intrinsic AHE, we can rewrite the anomalous Hall coefficient as $R_S = S_H \rho^2(T,H)$ with S_H as an H independent constant [27] and fit our $\rho_{yx}(H)$ traces well in $T_A < T \leqslant T_C$. The fitting parameters R_H and S_H are plotted in Fig. 4(b). The effective carrier density derived from R_H in $T > T_A$ is found to be 9×10^{20} holes/cm^3. It is consistent with the value found above T_C at 200 K where the Hall signal recovers almost a linear H dependence.

In $T < T_A$ however, this analysis is no longer valid and cannot capture the concave H dependence, even when an additional extrinsic contribution term is included. As seen in Fig. 4(c), the emergence of a novel H dependence below H_p^c replaces the gradual reduction of the AHE contribution. It is hard to connect it with the AHE picture as it bears no resemblance to $M(H)$. We rule out the possibility that this behavior is caused by the THE [2,3] for the following reasons: First, the T dependence—occurring at low T's and vanishing as T increases—is the opposite to what was observed in the THE in other magnetic systems [28]. Second, a recent neutron-scattering study could not identify the existence of a complex periodic spin structure of skyrmions [22].

It is interesting to compare the Hall effect of $Cr_{1/3}NbS_2$ to that of $Fe_{1/4}TaS_2$, an anisotropic magnetic dichalcogenide with a similar crystalline structure. Both have the same resistivity at 5 K, but $Cr_{1/3}NbS_2$ has one-tenth the carrier density of $Fe_{1/4}TaS_2$. This means the $Cr_{1/3}NbS_2$ has a tenfold larger mean-free path (l). The intrinsic AHE signal scales with $1/l^2$ and diminishes rapidly as T is lowered and ρ decreases [27], resulting in the OHE dominating the Hall signal at low temperatures, i.e., a recovery of H linear dependence of ρ_{yx}. This is consistent with our observation that the extrinsic AHE is negligible over the entire temperature range in $Cr_{1/3}NbS_2$ [31].

The fact that an unusual H profile of ρ_{yx} and the larger amplitude of out-of-plane AMR occur in the same T range $T < T_A \approx 50$ K implies that the two phenomena share a similar origin. In this temperature regime R_H, which was estimated from the slope of ρ_{yx} when $H > 3$ T, increases rapidly. The crossover temperature T_A also appeared in other measurements: The T dependence of the thermopower [29] changes slowly just below T_C and then after a broad shoulder around 50 K rapidly decreases. These unusual spin-orientation dependent transport features, unique to $Cr_{1/3}NbS_2$, emerge only below T_A. T_A is also consistent with a deviation from Bloch's $T^{3/2}$ law of $M(T)$ [13]. These observations point to a spin-orbit coupling effect of order $k_B T_A$ with k_B as the Boltzmann constant.

In an attempt to understand these anisotropic magnetotransport properties, first-principles calculations [32,33] were pursued (procedural details in Ref. [29]). Results of these calculations, depicted in Fig. 5, show a significant dependence of the calculated magnetic density of states on moment orientation, both for the total DOS (top) and the Cr DOS (bottom). As indicated in the inset to Fig. 5 for states very near the Fermi level (E_F)—less than 25 meV from E_F—the DOS can vary by as much as 15% depending on moment orientation. Moreover, the Fermi-level DOS was found to be 3.2% greater when the moments orient along the c axis instead of perpendicular to it, whereas the in-plane plasma frequencies

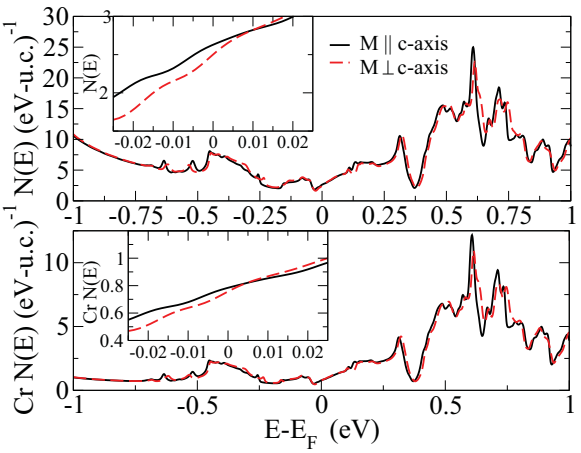

FIG. 5. (Color online) The calculated magnetic density of states of $Cr_{1/3}NbS_2$ per unit cell (u.c.) for the indicated magnetic moment orientations (a) total DOS and (b) Cr DOS. The energy scale ±25 meV centered at Fermi energy E_F is magnified in the insets. The DOS at E_F was found to be 3.2% greater when the moments orient along the c axis instead of perpendicular to it, whereas the in-plane plasma frequencies are essentially unaffected by magnetization orientation, which is consistent with enhanced conductivity within an order of unity.

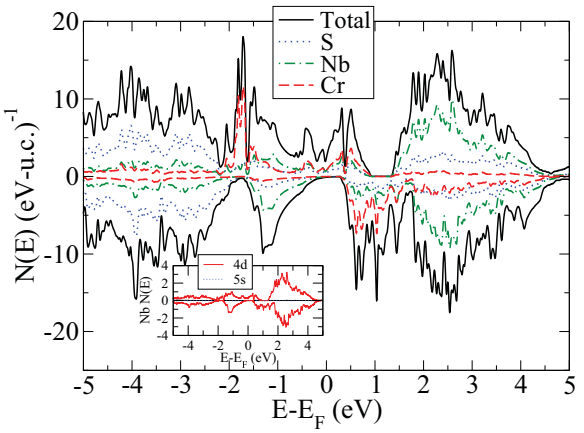

FIG. 6. (Color online) The calculated magnetic density of states of $Cr_{1/3}NbS_2$ projected by spin and atomic characters. The inset: the orbital-projected character of the Nb DOS.

are essentially unaffected by magnetization orientation. Thus, neglecting spin-orientation dependent scattering processes, the increase in DOS is largely responsible for the reduction of the in-plane resistivity when the magnetization lies parallel to the c axis instead of the ab plane. The resistivities for the two spin-polarization directions at 5 K differ by 11%, which is bigger than the DOS difference by a factor of the order of unity. Also, by examining the bands near E_F (within a 20-meV window) for both orientations, one finds the averaged offset in the energies to be approximately 1.7 meV $\simeq$ 20 K. This is a direct result of SOC and consistent with the temperature scale T_A found in the MR and Hall effect data. These changes in electronic structure and their subsequent modification of scattering processes are likely responsible for the spin-orientation dependence in the transport.

We note also from Fig. 5 that the Cr-site DOS is essentially of the same shape as the total DOS within an eV of E_F. In addition, the effects on the Cr DOS of the change in moment orientation from [001] ($\| c$) to [100] ($\| ab$) closely parallel the changes in the total DOS. This is due to the primary role of the Cr atoms in the magnetic behavior—only for atoms with a large local moment, such as Cr here, does one expect a moment-orientation dependent DOS. Note that in the calculation the induced Nb moment is only $0.05\mu_B$ and that on S is essentially zero.

In Fig. 6 we show the magnetic state DOS projected into spin-up and spin-down sub-bands, along with the Nb 4d and 5s orbital-projected DOS. A substantial exchange splitting is visible in the Cr DOS as expected given its magnetic character with some minor splitting also observed in Nb and S. There is little, if any, spin-down character to the Cr DOS for nearly 2 eV below E_F. This is suggestive of the strength of the magnetism in this system as indicated by the $3\mu_B$/Cr total magnetic moment found both in the calculation and in the experiment. There is substantial hybridization around E_F, indicative of covalent bonding, although the Cr states are generally confined to within 2 eV of E_F and Nb and S predominate outside this range. In the inset of Fig. 6 we plot the orbital-projected Nb DOS, which is dominated by 4d contributions with the 5s contribution negligible.

Further detailed investigation on the electronic structure depending on the spin direction will shed light on understanding the difference in amplitudes of in-plane and out-of-plane AMRs. This mechanism is suspected to be closely related to the abnormal H dependence of the Hall effect observed for $T < T_A$.

The remarkable sensitivity of the magnetotransport behavior to polarized spin orientation in $Cr_{1/3}NbS_2$ is mostly driven by Cr^{3+} ions. Strong magnetization orientation dependence of the electronic structure of 3d metals leads to large effects on the magnetotransport properties in $Cr_{1/3}NbS_2$. The same strong dependence also underlies efforts to control magnetic anisotropy in multilayer systems made of 3d magnetic elements. Our results demonstrate a closely interwoven relation among the orientation of magnetization, the resultant electronic structure change, and its influence on the electrical conduction, all of which are mediated by spin-orbit coupling. Furthermore, the noncollinear helical ground state enriches the role of spin-orbit coupling and the subsequent complexity of the electrical transport properties.

ACKNOWLEDGMENTS

The authors thank J. G. Checkelsky, X. Fan, M. Hermele, and K. M. McElroy for enlightening discussions. This work at CU was supported by the U.S. Department of Energy, Office of Science, Basic Energy Sciences under Award No. DE-SC0006888, and at ORNL by DOE, Office of Science BES, Materials Sciences and Engineering Division. D.S.P. was supported by the Critical Materials Institute, an Energy Innovation Hub funded by the U.S. DOE, Energy Efficiency and Renewable Energy, Advanced Manufacturing Office.

[1] S. Muhlbauer, B. Binz, F. Jonietz, C. Pfleiderer, A. Rosch, A. Neubauer, R. Georgii, and P. Boni, Science **323**, 915 (2009).

[2] M. Lee, W. Kang, Y. Onose, Y. Tokura, and N. P. Ong, Phys. Rev. Lett. **102**, 186601 (2009).

[3] A. Neubauer, C. Pfleiderer, B. Binz, A. Rosch, R. Ritz, P. G. Niklowitz, and P. Böni, Phys. Rev. Lett. **102**, 186602 (2009).

[4] I. Dzyaloshinsky, J. Phys. Chem. Solids **4**, 241 (1958).

[5] T. Moriya, Phys. Rev. **120**, 91 (1960).

[6] J. M. Hopkinson and H.-Y. Kee, Phys. Rev. B **79**, 014421 (2009).

[7] A. Fert, V. Cros, and J. Sampaio, Nat. Nanotechnol. **8**, 152 (2013).

[8] N. Romming, C. Hanneken, M. Menzel, J. E. Bickel, B. Wolter, K. von Bergmann, A. Kubetzka, and R. Wiesendanger, Science **341**, 636 (2013).

[9] B. C. Sales, R. Jin, and D. Mandrus, Phys. Rev. B **77**, 024409 (2008).

[10] Y. Mokrousov, H. Zhang, F. Freimuth, B. Zimmermann, N. H. Long, J. Weischenberg, I. Souza, P. Mavropoulos, and S. Blügel, J. Phys.: Condens. Matter **25**, 163201 (2013).

[11] N. J. Ghimire, M. A. McGuire, D. S. Parker, B. Sipos, S. Tang, J.-Q. Yan, B. C. Sales, and D. Mandrus, Phys. Rev. B **87**, 104403 (2013).

[12] T. Moriya and T. Miyadai, Solid State Commun. **42**, 209 (1982).

[13] T. Miyadai, K. Kikuchi, H. Kondo, S. Sakka, M. Arai, and Y. Ishikawa, J. Phys. Soc. Jpn. **52**, 1394 (1983).

[14] Y. Togawa, T. Koyama, K. Takayanagi, S. Mori, Y. Kousaka, J. Akimitsu, S. Nishihara, K. Inoue, A. S. Ovchinnikov, and J. Kishine, Phys. Rev. Lett. **108**, 107202 (2012).

[15] Y. Togawa, Y. Kousaka, S. Nishihara, K. Inoue, J. Akimitsu, A. S. Ovchinnikov, and J. Kishine, Phys. Rev. Lett. **111**, 197204 (2013).

[16] H. Brooks, Phys. Rev. **58**, 909 (1940).

[17] P. Bruno, Phys. Rev. B **39**, 865 (1989).

[18] D.-s. Wang, R. Wu, and A. J. Freeman, Phys. Rev. B **47**, 14932 (1993).

[19] M. Bode, S. Heinze, A. Kubetzka, O. Pietzsch, X. Nie, G. Bihlmayer, S. Blügel, and R. Wiesendanger, Phys. Rev. Lett. **89**, 237205 (2002).

[20] F. Gimbert and L. Calmels, Phys. Rev. B **86**, 184407 (2012).

[21] K. Hotta, K. Nakamura, T. Akiyama, T. Ito, T. Oguchi, and A. J. Freeman, Phys. Rev. Lett. **110**, 267206 (2013).

[22] N. J. Ghimire, Ph.D. thesis, University of Tennessee, 2013.

[23] T. G. S. M. Rijks, S. K. J. Lenczowski, R. Coehoorn, and W. J. M. de Jonge, Phys. Rev. B **56**, 362 (1997).

[24] A. Kobs, S. Heße, W. Kreuzpaintner, G. Winkler, D. Lott, P. Weinberger, A. Schreyer, and H. P. Oepen, Phys. Rev. Lett. **106**, 217207 (2011).

[25] T. McGuire and R. Potter, IEEE Trans. Magn. **11**, 1018 (1975).

[26] B. J. Chapman, A. Bornstein, N. J. Ghimire, D. Mandrus, and M. Lee, Appl. Phys. Lett. **105**, 072405 (2014).

[27] M. Lee, Y. Onose, Y. Tokura, and N. P. Ong, Phys. Rev. B **75**, 172403 (2007).

[28] B. J. Chapman, M. G. Grossnickle, T. Wolf, and M. Lee, Phys. Rev. B **88**, 214406 (2013).

[29] See Supplemental Material at http://link.aps.org/supplemental/10.1103/PhysRevB.91.184401 for thermopower measurement, out-of-plane AMR, and details of first-principle calculations.

[30] M. N. Baibich, J. M. Broto, A. Fert, F. Nguyen Van Dau, F. Petroff, P. Etienne, G. Creuzet, A. Friederich, and J. Chazelas, Phys. Rev. Lett. **61**, 2472 (1988).

[31] The second term $\rho_{yx} = \mu_0 R_H H + \mu_0 R_s M$ was modified to $\mu_0 S_H \rho^2 M(1 + \frac{\rho_I}{\rho})$ with ρ_I as an additional fitting parameter, but fits revealed $\frac{\rho_I}{\rho} \ll 1$ over most of the T range investigated. Meanwhile, in $Fe_{1/4}TaS_2$, ρ_{xy} is dictated by the intrinsic AHE at low T and then the extrinsic AHE as T approaches T_C.

[32] P. Blaha, K. Schwarz, G. Madsen, D. Kvasnicka, and J. Luitz, WIEN2k, *An Augmented Plane Wave + Local Orbitals Program for Calculating Crystal Properties* (Karlheinz Schwarz, Techn. Universität Wien, Austria, 2001).

[33] J. P. Perdew, K. Burke, and M. Ernzerhof, Phys. Rev. Lett. **78**, 1396 (1997).